Rapid Communications

Competition between spin-orbit coupling, magnetism, and dimerization in the honeycomb iridates: α-Li_2IrO_3 under pressure

V. Hermann,[1] M. Altmeyer,[2] J. Ebad-Allah,[1,3] F. Freund,[4] A. Jesche,[4] A. A. Tsirlin,[4] M. Hanfland,[5] P. Gegenwart,[4] I. I. Mazin,[6] D. I. Khomskii,[7] R. Valentí,[2,*] and C. A. Kuntscher[1,†]

[1]*Experimentalphysik II, Augsburg University, 86159 Augsburg, Germany*
[2]*Institut für Theoretische Physik, Goethe-Universität Frankfurt, 60438 Frankfurt am Main, Germany*
[3]*Department of Physics, Tanta University, 31527 Tanta, Egypt*
[4]*Experimentalphysik VI, Center for Electronic Correlations and Magnetism, Augsburg University, 86159 Augsburg, Germany*
[5]*European Synchrotron Radiation Facility (ESRF), Boîte Postale 220, 38043 Grenoble, France*
[6]*Code 6393, Naval Research Laboratory, Washington DC 20375, USA*
[7]*II. Physikalisches Institut, Universität zu Köln, 50937 Köln, Germany*

(Received 5 December 2017; published 31 January 2018)

Single-crystal x-ray diffraction studies with synchrotron radiation on the honeycomb iridate α-Li_2IrO_3 reveal a pressure-induced structural phase transition with symmetry lowering from monoclinic to triclinic at a critical pressure of $P_c = 3.8$ GPa. According to the evolution of the lattice parameters with pressure, the transition mainly affects the *ab* plane and thereby the Ir hexagon network, leading to the formation of Ir-Ir dimers. These observations are independently predicted and corroborated by our *ab initio* density functional theory calculations where we find that the appearance of Ir-Ir dimers at finite pressure is a consequence of a subtle interplay between magnetism, correlation, spin-orbit coupling, and covalent bonding. Our results further suggest that at P_c the system undergoes a magnetic collapse. Finally we provide a general picture of competing interactions for the honeycomb lattices A_2MO_3 with A = Li, Na and M = Ir, Ru.

DOI: 10.1103/PhysRevB.97.020104

In recent years, layered honeycomb 4*d* and 5*d* metal oxides, such as Na_2IrO_3, α-Li_2IrO_3, and α-$RuCl_3$, with d^5 electronic occupation, have been intensively scrutinized as Kitaev physics candidates [1–7] due to the presence of sizable nearest-neighbor bond-dependent Ising interactions between effective spin-1/2 local moments. However, instead of the expected Z_2 spin liquid ground state, as shown by Kitaev [1], these materials order magnetically either in a zigzag structure [4,8–10] (Na_2IrO_3, α-$RuCl_3$) or an incommensurate spiral structure [11] (α-Li_2IrO_3). This magnetic long-range order has been suggested to originate from further non-Kitaev interactions and a present debate is whether the magnetic excitations in these materials nevertheless retain some of the nontrivial features of the Kitaev model, such as fractionalization [10,12,13]. It might be expected that one route to enhance Kitaev interactions would be by applying pressure or by doping. However, the physics of this structural family is much richer and there are many more instabilities that interfere with the Kitaev interactions, in particular under pressure. Indeed, Li_2RuO_3 with Ru in a $4d^4$ electronic configuration is nonmagnetic and strongly dimerized at ambient pressure [14–16], while $SrRu_2O_6$ with Ru in a $4d^3$ configuration is an ultrahigh-temperature antiferromagnet [17,18], despite having the same planar geometry, and shows no bond disproportionation.

Many factors control the competition between Kitaev physics, magnetism, and dimerization [19] in A_2MO_3 honeycomb networks, such as the number of transition-metal M d electrons, the strength of spin-orbit coupling, the strength of correlation effects and Hund's rule coupling, or the ionic radii of the buffer element A. In this context it is particularly instructive to compare α-Li_2IrO_3 with Li_2RuO_3, which contains the same buffer element (Li). α-Li_2IrO_3 is less correlated than Li_2RuO_3 (5*d* versus 4*d* electrons, respectively) so that one would expect in the former a reduced tendency to magnetism in favor of dimerization. On the other hand, α-Li_2IrO_3 has only a single hole in the t_{2g} manifold, as opposed to two in Li_2RuO_3, and stronger spin-orbit interaction. This should weaken dimerization and strengthen Kitaev-type physics in α-Li_2IrO_3. Further, in comparison to Na_2IrO_3, the Li ionic radius is smaller than the Na ionic radius, thus favoring dimerization in Li_2MO_3. The result is a delicate balance of all these effects. At ambient pressure, α-Li_2IrO_3 shows a highly symmetric honeycomb structure with a bond disproportionation of less than 3% and magnetically orders in a spiral structure, which features a noncollinear incommensurate antiferromagnetic order inside the Ir planes [11]. It is not unreasonable to assume that α-Li_2IrO_3 may be an intermediate case between Na_2IrO_3 and Li_2RuO_3, and could be switched between the two extremes (magnetic Kitaev and nonmagnetic dimerized) by an external perturbation, such as physical pressure, an intriguing possibility.

In this work, we show that this is indeed the case. We find that, in contrast to Na_2IrO_3, in Li_2IrO_3 a structural phase transition from a monoclinic to a dimerized triclinic structure occurs at a low pressure of $P_c = 3.8$ GPa. Density functional theory (DFT) calculations also find this transition, with the transition

*valenti@th.physik.uni-frankfurt.de
†christine.kuntscher@physik.uni-augsburg.de

 ©2018 American Physical Society

pressure depending on the assumed correlation strength. The experimental P_c is obtained for an effective Hubbard repulsion interaction $U - J = 1.5$ eV (U and J being the Hubbard and Hund's rule coupling parameters, respectively), which is very reasonable for a $5d$ metal. Analyzing the calculations we observe that indeed α-Li_2IrO_3 is a borderline case, wherein the singlet dimerized solution and the magnetic undimerized one are very close in energy. Pressure reduces the tendency to magnetism, thus diminishing the energetic advantage of forming an antiferromagnetic state, and brings Ir ions closer together, enhancing the advantage of forming covalent bonds. Compared to Li_2RuO_3, the main difference lies in the fact that in α-Li_2IrO_3 only one d hole participates in the formation of covalent bonds.

At ambient pressure α-Li_2IrO_3 crystallizes in a monoclinic $C2/m$ space group [20,21], with the unit cell shown in the Supplemental Material [22]. Ir forms hexagons with edge-sharing IrO_6 octahedra and a single Li atom in its center (Ir_2LiO_3 layer). These layers are intercalated with Li_3O_3 layers. At ambient pressure all Ir-Ir bonds have nearly the same length.

The pressure dependence of the lattice parameters obtained by refining the single-crystal x-ray diffraction (XRD) data is depicted in Figs. 1(a) and 1(b). See the Supplemental Material [22] for a description of sample preparation and pressure-dependent XRD measurements. For pressures up to ≈3.8 GPa the lattice parameters decrease monotonically with increasing pressure. We included $b' = b/\sqrt{3}$ for a better comparison between the three lattice parameters. Both in-plane lattice parameters a and b' are affected in a very similar manner. The strongest effect is observed for the lattice parameter c. This is illustrated by the c/a value in the inset of Fig. 1(a), which decreases with pressure up to 3.8 GPa. Within the error bar the monoclinic angle β is not affected by pressure.

For pressures above $P_c = 3.8$ GPa the crystal structure can no longer be refined within the $C2/m$ space group, but requires a triclinic group, $P\bar{1}$, with half of the unit cell volume. The structural phase transition is completely reversible [see open symbols in Figs. 1(a) and 1(b)]. In order to compare the high-pressure evolution of the lattice parameters to the low-pressure structures, we consider a supercell, isometric to the ambient-pressure unit cell. Note that due to the triclinic symmetry group, two different choices are possible. We select one of these (resulting in the $X1$ dimerization discussed below) and show the refined lattice parameters of this doubled triclinic unit cell in Figs. 1(a) and 1(b). All angles of this cell exhibit an anomaly at P_c: γ jumps from 90° to ≈93.4° and is independent of pressure above P_c within the error bars, while α monotonically decreases with pressure, and β exhibits an abrupt but small (≈1°) decrease at P_c and then monotonically increases with pressure. The structural phase transition also induces abrupt changes in the lattice parameters. Whereas the in-plane lattice parameter a is most affected with an overall reduction of about 3%, the in-plane lattice constant b slightly increases at P_c. Interestingly, at the transition the c/a ratio jumps up from ≈0.99 to 1.01, but above it monotonically decreases with pressure. Thus, also above P_c the lattice is more compressible along the c direction.

We fitted the volume V and the lattice parameters r (r=a,b,c) separately for the low- and high-pressure phases

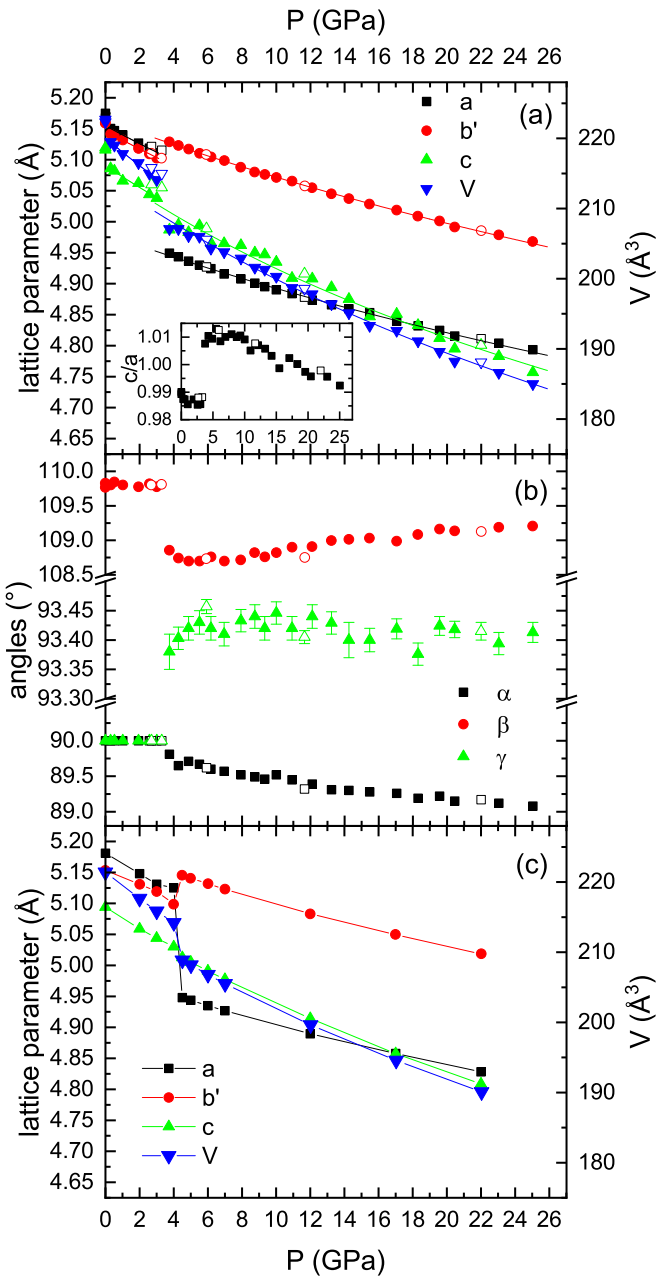

FIG. 1. Pressure dependence of the volume V of the unit cell and the lattice parameters a, $b' = b/\sqrt{3}$, c, and c/a value shown in (a) and the corresponding angles α, β, and γ in (b). For a better comparison a nonprimitive unit cell was used for the high-pressure phase above 3.8 GPa, as explained in the text. The solid lines in (a) are fits with a Murnaghan-type equation of state (see text). Open symbols are values observed during pressure release. If not shown, the error bar is smaller than the symbol size. (c) Calculated lattice parameters for pressures up to 22 GPa (corrected by 3 GPa to closely resemble the experimental crystal volume at zero pressure).

with the second-order Murnaghan equation of state [23], to obtain the bulk moduli $B_{0,V}$ and $B_{0,r}$:

$$V(p) = V_0[(B_0'/B_{0,V})p + 1]^{-1/B_0'}, \quad (1)$$

$$r(p) = r_0[(B_0'/B_{0,r})p + 1]^{-1/3B_0'} \quad (2)$$

TABLE I. Bulk moduli $B_{0,V}$ and $B_{0,r}$ with $r=a,b,c$ of α-Li_2IrO_3 in the low-pressure (low-p) and high-pressure (high-p) phase, as obtained from fitting the volume V and individual lattice parameters with a Murnaghan-type equation of state, with B_0' set to 4. Corresponding values for Na_2IrO_3 were obtained from corresponding fits of the data given in Ref. [24].

	$B_{0,V}$	V_0 (Å^3)	$B_{0,a}$ (GPa)	$B_{0,b}$ (GPa)	$B_{0,c}$ (GPa)
Low-p phase	106(5)	220.1(2)	114(2)	113(2)	92(11)
High-p phase	125(3)	214.3(9)	167(2)	166(2)	86(5)
Na_2IrO_3	100.6(1)	269.55(3)	152(2)	146 (2)	58(1)

with B_0' fixed to 4. The results are summarized in Table I. For the low-pressure phase we find $B_{0,V} \approx 106(5)$ GPa. The bulk moduli $B_{0,a}$ and $B_{0,b}$ are almost the same, while $B_{0,c}$ is lower, confirming that α-Li_2IrO_3 is more compressible along the c direction. Above P_c the bulk modulus is increased to $B_{0,V} \approx 125(3)$ GPa, while $B_{0,a}$ and $B_{0,b}$ sharply increase to ≈170 GPa, and $B_{0,c}$ is slightly decreased compared to the low-pressure phase to about 86(5) GPa. Thus, α-Li_2IrO_3 hardens at P_c, and the hardening takes place within the Ir planes.

For a comparison with isostructural Na_2IrO_3 we refitted the data of Ref. [24] with B_0' fixed to 4 and list the so-obtained results in Table I. Compared to α-Li_2IrO_3 in the low-pressure phase, the bulk modulus $B_{0,V}$ of Na_2IrO_3 is only slightly lower. Interestingly, for Na_2IrO_3 the values $B_{0,a}$ and $B_{0,b}$ are much higher, whereas $B_{0,c}$ is much lower. Hence, in its low-pressure phase α-Li_2IrO_3 is more compressible in the ab plane and less compressible along the c direction as compared to Na_2IrO_3. The former effect could be attributed to the smaller Li atoms occupying the center of the hexagons (instead of Na), and the latter to the stronger Li-O bonds with strong out-of-ab-plane character [24]. The higher in-plane compressibility is instrumental in triggering Ir dimerization. Above P_c the bulk moduli $B_{0,a}$ and $B_{0,a}$ of α-Li_2IrO_3 are sharply enhanced and become similar to those for Na_2IrO_3, i.e., the compressibility of the ab plane becomes similar for both compounds.

For a more detailed investigation, we refined the Ir-Ir bond lengths [see Fig. 2(a)], since they are relevant for the magnetic and electronic properties of the material [7,25,26]. In a perfectly hexagonal lattice one can distinguish three Ir-Ir bonds related by a 120° rotation [Fig. 2(b)]. Following the nomenclature of Ref. [26], we shall call them $Z1$, $X1$, and $Y1$. In the monoclinic phase below P_c, the $X1$ and $Y1$ bonds are equivalent by symmetry, while $Z1$ is distinct. The high-pressure phase lacks the C_2 symmetry, and therefore the two bonds $X1$ and $Y1$ become inequivalent. The Ir-Ir bond lengths as a function of pressure, as obtained from the refinement of the XRD data, are plotted in Fig. 2(a). At P_c one of the $X1/Y1$ bonds is slightly increased from ≈2.95 Å to ≈3.00 Å, while the other one is *strongly decreased* to 2.69 Å. Note that this distance is smaller than the Ir-Ir distance of 2.714 Å in Ir metal. As opposed to Li_2RuO_3, where (i) the dimerized bonds alternate between $X1$ and $Y1$, (ii) a C_2 axis is preserved and (iii) the $P2_1/m$ monoclinic symmetry is realized, in α-Li_2IrO_3 either $X1$ or $Y1$ bonds dimerize, thus breaking the C_2 symmetry [Figs. 2(c) and 2(d)]. The $Z1$ bond's length increases at P_c and becomes nearly degenerate with that

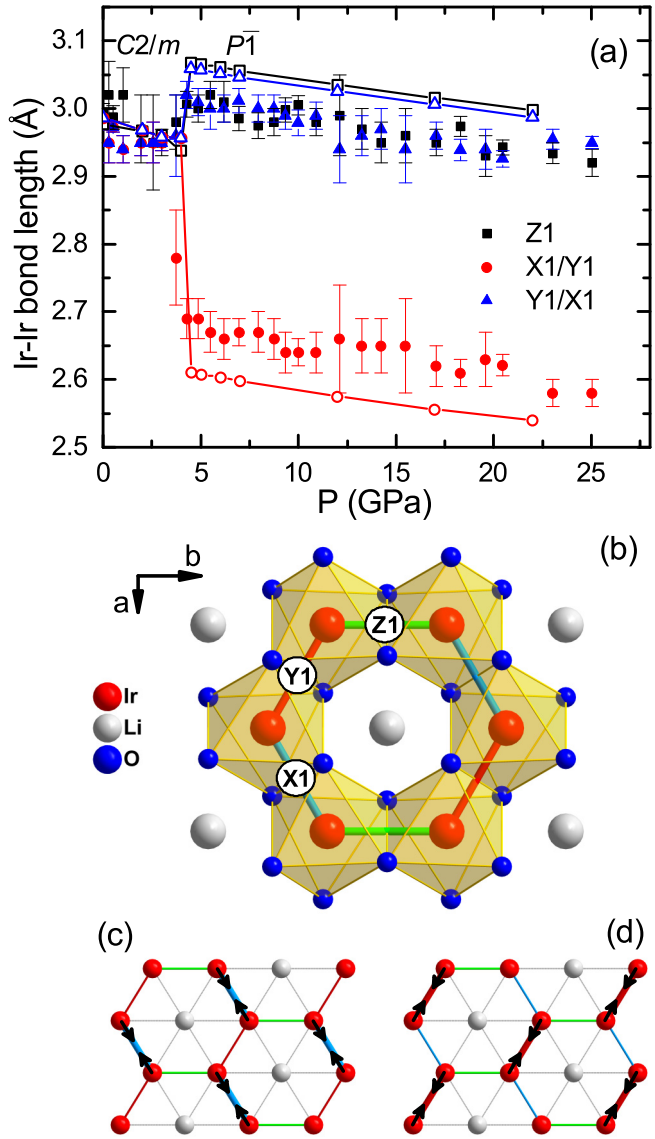

FIG. 2. (a) Pressure dependence of the Ir-Ir distances for the Ir hexagons in the ab plane, with the nomenclature (Ir bonds $X1$, $Y1$, $Z1$) given in (b) for the ambient-pressure monoclinic crystal structure. Ir-Ir bond lengths as predicted from our relaxations are shown as open symbols connected by a line. The two equivalent ordering patterns of the Ir-Ir dimers above P_c are illustrated in (c) and (d).

of the longer $X1/Y1$ bond. The energy difference between these various types of dimerization is related to different mutual arrangements of the dimers: armchair (herringbone) or ladder (parallel). As discussed in Refs. [16,27] the choice is being made by long-range, likely elastic, interactions. It is worth noting that very recently Veiga *et al.* [28] reported a similar structural phase transition at $P_c \approx 4$ GPa in β-Li_2IrO_3.

In order to gain more insight into the physics of dimerization and interactions that control it, we have performed first-principles DFT calculations, as described in the Supplemental Material [22]. First, we find, in agreement with experiment and qualitative considerations, that α-Li_2IrO_3 is more prone to dimerization than Na_2IrO_3, and, in fact, dimerizes in DFT

within the generalized gradient approximation (GGA) already at zero pressure. This can be traced to the underestimation of correlation effects, and therefore underestimation of the tendency to magnetism. Indeed, Ref. [29] showed that at the mean-field level, usually called the LDA + U approximation (or GGA + U), correlations increase the Stoner coupling I, which characterizes the tendency to form magnetic moments in DFT, as $I \rightarrow I + (U - J)/5$, where U and J are the Hubbard and Hund's rule coupling parameters. For 5d metals I is of the order of 0.3 eV, while $U_{\text{eff}} = U - J$, as we discuss in more detail in the Supplemental Material [22], should be taken to be close to 1.5 eV. Thus, including correlations enhances the Stoner coupling by about a factor of 2.

Furthermore, in accordance with our previous study [30] for the isoelectronic doping series $Na_{(2-x)}Li_xIrO_3$, we find that at ambient pressure, using the experimental crystal volume, it is not enough to include an effective Hubbard correlation of about $U_{\text{eff}} = U - J = 1.5$ eV to stabilize magnetism and the observed undimerized structure. The spin-orbit coupling also appears essential. Here we choose the zigzag antiferromagnetic order to mimic the incommensurate spiral order [31] observed in experiment [11]. This indicates that the observed structural transition at finite pressures is driven by two competing energy scales: (i) the energy gained by the formation of magnetic moments and (ii) the energy gained by placing two electrons of neighboring Ir atoms in the bonding orbital resulting from the Ir-Ir dimerization. In both processes, correlation effects are significantly involved. At low pressures the overlap of adjacent Ir atoms is slightly too small to favor the dimerization, while a small decrease of the Ir-Ir distances with pressure changes the situation and results in a breakdown of the magnetic order and structural dimerization. Note that in the above-mentioned experiment on β-Li_2IrO_3 [28,32] ferromagnetic polarization disappeared already at $P_m \sim 2$ GPa prior to the putative dimerization transition, and one can speculate that at a higher pressure, corresponding to dimerization, the local moments collapse as well, in agreement with the present calculations. Alternatively, between P_m and P_c the system may be in a valence bond liquid state, similar to that in Li_2RuO_3 at high temperature [16]. It is furthermore interesting to note that also in the stripy honeycomb γ-Li_2IrO_3 the ambient-pressure incommensurate magnetic order was observed to disappear under compression, without accompanying change in lattice symmetry [33].

In Fig. 1(c) we show the lattice parameters calculated within relativistic GGA + U as a function of the simulated hydrostatic pressures. As typical for GGA, we observe slight underbinding, so that the experimental volume at ambient pressure corresponds to the calculated pressure of ≈3 GPa. In the following, we subtract this systematic error from the calculated pressure. With this in mind, the calculated transition pressure as well as the resulting bond disproportionations are in good agreement with the experiment. At the phase transition, the $X1/Y1$ dimerized structure is the most stable with a relative Ir-Ir dimerization of long/short bond $=3.07/2.61 \approx 1.18$ in very good agreement with the experiment, as shown in Fig. 2(a). In addition, we find an abrupt collapse of magnetism at P_c (see Supplemental Material [22]).

At this point, it is insightful to investigate the dimerization pressure for the closely related Na_2IrO_3 compound. In fact, at 29 GPa the crystal structure of Na_2IrO_3 has been shown to resemble that of α-Li_2IrO_3 with respect to the lattice metrics [24]. Our simulations for Na_2IrO_3 (see Supplemental Material [22]) predict lattice parameters that are in excellent agreement with the observations in the experimentally studied pressure range up to 30 GPa. At about 45 GPa, we find a structural transition perfectly analogous to the one we observed in α-Li_2IrO_3. It is accompanied by a magnetic collapse and the Ir-Ir dimerization triggers a strong decrease of the in-plane a lattice parameter, while the b-lattice parameter is slightly enhanced. The c parameter in Na_2IrO_3 is significantly larger than in α-Li_2IrO_3, due to the larger intercalated ion in Na_2IrO_3. Notably, the Ir-Ir distance, at which the transition occurs, about 2.95 Å, is almost exactly the same as for α-Li_2IrO_3 and also the unit cell volume is remarkably similar ($V \approx 210$ Å^3). Indeed, due to the larger Na ion size compared to Li, the IrO_2 layer is less compressible in Na_2IrO_3, as discussed above, and thus formation of sufficiently short dimers (in order to take full advantage of the covalent energy) is hindered. This is also validated by our bulk modulus study (Table I). Otherwise, as expected due to their similar electronic properties, these two compounds behave in the same way. A similar argument holds for the compounds Na_2RuO_3 and Li_2RuO_3, since Na_2RuO_3 is not dimerized at ambient pressure [34], whereas Li_2RuO_3 is. The pressure of ≈45 GPa, at which we expect the dimerization transition in Na_2IrO_3 to occur, should be accessible in diamond-anvil cells but is beyond the scope of the present study. Conducting such an experiment in the future will be invaluable to confirm the general physical picture that we deduce in this Rapid Communication.

In summary, α-Li_2IrO_3 undergoes a pressure-induced structural phase transition at $P_c = 3.8$ GPa with symmetry lowering to $P\bar{1}$. This transition mainly affects the ab plane with the Ir hexagons. As corroborated by our density functional theory calculations, our refinements of the Ir positions show that the structural phase transition is accompanied by a dimerization of the previously equally long $X1/Y1$ Ir-Ir bonds. Analysis of the total energies of the high-symmetry and the dimerized $P\bar{1}$ lattices at the experimental crystal volume shows that several factors affect the propensity to dimerization, namely, the size of the central ion (i.e., Li vs Na), as well as the strength of the spin-orbit interaction, electronic correlations, and Hund's rule coupling (all of them discourage dimerization; cf. 4d vs 5d metals), and the number of d electrons in the metal species (e.g., Ru vs Ir). Li_2RuO_3, having (a) a small central ion, (b) four d electrons, and (c) weaker spin-orbit coupling has the strongest tendency toward dimerization among the known 213 systems, despite being more magnetic than Ir. α-Li_2IrO_3 has one more d electron and stronger spin-orbit interaction, but weaker Hubbard and Hund's rule couplings, and thus dimerizes only under pressure, albeit at a relatively small P_c. Na_2IrO_3 only differs in terms of the central ion size, and thus compressibility, and is predicted to dimerize as well, at an accessible, but much higher pressure.

We thank the ESRF, Grenoble, France, for the provision of beamtime. This work was financially supported by the Federal Ministry of Education and Research (BMBF), Germany, through Grant No. 05K13WA1 (Verbundprojekt 05K2013,

Teilprojekt 1, PT-DESY). D.I.Kh. is grateful to D. Haskel for useful discussions. R.V. acknowledges fruitful discussions with Y. Singh. M.A., D.I.Kh., R.V., and P.G. acknowledge financial support by the Deutsche Forschungsgemeinschaft (DFG), Germany, through TRR 80, SPP 1666, TRR 49, and SFB 1238. A.J. acknowledges support from the DFG through Grant No. JE 748/1. A.A.T. acknowledges financial support from the Federal Ministry for Education and Research via the Sofja-Kovalevskaya Award of Alexander von Humboldt Foundation, Germany. I.I.M. was supported by A. von Humboldt Foundation and by ONR through the NRL basic research program.

[1] A. Kitaev, Anyons in an exactly solved model and beyond, Ann. Phys. (NY) **321**, 2 (2006).

[2] G. Jackeli and G. Khaliullin, Mott Insulators in the Strong Spin-Orbit Coupling Limit: From Heisenberg to a Quantum Compass and Kitaev Models, Phys. Rev. Lett. **102**, 017205 (2009).

[3] J. Chaloupka, G. Jackeli, and G. Khaliullin, Kitaev-Heisenberg Model on a Honeycomb Lattice: Possible Exotic Phases in Iridium Oxides A_2IrO_3, Phys. Rev. Lett. **105**, 027204 (2010).

[4] S. K. Choi, R. Coldea, A. N. Kolmogorov, T. Lancaster, I. I. Mazin, S. J. Blundell, P. G. Radaelli, Yogesh Singh, P. Gegenwart, K. R. Choi, S.-W. Cheong, P. J. Baker, C. Stock, and J. Taylor, Spin Waves and Revised Crystal Structure of Honeycomb Iridate Na_2IrO_3, Phys. Rev. Lett. **108**, 127204 (2012).

[5] K. W. Plumb, J. P. Clancy, L. J. Sandilands, V. Vijay Shankar, Y. F. Hu, K. S. Burch, Hae-Young Kee, and Young-June Kim, α-$RuCl_3$: A spin-orbit assisted Mott insulator on a honeycomb lattice, Phys. Rev. B **90**, 041112(R) (2014).

[6] S. H. Chun, J.-W. Kim, J. Kim, H. Zheng, C. C. Stoumpos, C. D. Malliakas, J. F. Mitchell, K. Mehlawat, Y. Singh, Y. Choi, T. Gog, A. Al-Zein, M. Moretti Sala, M. Krisch, J. Chaloupka, G. Jackeli, G. Khaliullin, and B. J. Kim, Direct evidence for dominant bond-directional interactions in a honeycomb lattice iridate Na_2IrO_3, Nat. Phys. **11**, 462 (2015).

[7] S. M. Winter, A. A. Tsirlin, M. Daghofer, J. van den Brink, Yogesh Singh, P. Gegenwart, and R. Valentí, Models and materials for generalized Kitaev magnetism, J. Phys.: Condens. Matter **29**, 493002 (2017).

[8] R. D. Johnson, S. C. Williams, A. A. Haghighirad, J. Singleton, V. Zapf, P. Manuel, I. I. Mazin, Y. Li, H. O. Jeschke, R. Valentí, and R. Coldea, Monoclinic crystal structure of α-$RuCl_3$ and the zigzag antiferromagnetic ground state, Phys. Rev. B **92**, 235119 (2015).

[9] J. A. Sears, M. Songvilay, K. W. Plumb, J. P. Clancy, Y. Qiu, Y. Zhao, D. Parshall, and Young-June Kim, Magnetic order in α-$RuCl_3$: A honeycomb-lattice quantum magnet with strong spin-orbit coupling, Phys. Rev. B **91**, 144420 (2015).

[10] A. Banerjee, C. A. Bridges, J.-Q. Yan, A. A. Aczel, L. Li, M. B. Stone, G. E. Granroth, M. D. Lumsden, Y. Yiu, J. Knolle, S. Bhattacharjee, D. L. Kovrizhin, R. Moessner, D. A. Tennant, D. G. Mandrus, and S. E. Nagler, Proximate Kitaev quantum spin liquid behavior in a honeycomb magnet, Nat. Mater. **15**, 733 (2016).

[11] S. C. Williams, R. D. Johnson, F. Freund, S. Choi, A. Jesche, I. Kimchi, S. Manni, A. Bombardi, P. Manuel, P. Gegenwart, and R. Coldea, Incommensurate counterrotating magnetic order stabilized by Kitaev interactions in the layered honeycomb α-Li_2IrO_3, Phys. Rev. B **93**, 195158 (2016).

[12] S. M. Winter, K. Riedl, P. A. Maksimov, A. L. Chernyshev, A. Honecker, and R. Valentí, Breakdown of magnons in a strongly spin-orbital coupled magnet, Nat. Commun. **8**, 1152 (2017).

[13] Y. Kasahara, K. Sugii, T. Ohnishi, M. Shimozawa, M. Yamashita, N. Kurita, H. Tanaka, J. Nasu, Y. Motome, T. Shibauchi, and Y. Matsuda, Unusual thermal Hall effect in a Kitaev spin liquid candidate α-$RuCl_3$, arXiv:1709.10286.

[14] Y. Miura, Y. Yasui, M. Sato, N. Igawa, and K. Kakurai, New-type phase transition of Li_2RuO_3 with honeycomb structure, J. Phys. Soc. Jpn. **76**, 033705 (2007).

[15] J. Park, T.-Y. Tan, D. T. Adroja, A. Daoud-Aladine, S. Choi, D.-Y. Cho, S.-H. Lee, J. Kim, H. Sim, T. Morioka, H. Nojiri, V. V. Krishnamurthy, P. Manuel, M. R. Lees, S. V. Streltsov, D. I. Khomskii, and J.-G. Park, Robust singlet dimers with fragile ordering in two-dimensional honeycomb lattice of Li_2RuO_3, Sci. Rep. **6**, 25238 (2016).

[16] S. A. J. Kimber, I. I. Mazin, J. Shen, H. O. Jeschke, S. V. Streltsov, D. N. Argyriou, R. Valentí, and D. I. Khomskii, Valence bond liquid phase in the honeycomb lattice material Li_2RuO_3, Phys. Rev. B **89**, 081408(R) (2014).

[17] C. I. Hiley, D. O. Scanlon, A. A. Sokol, S. M. Woodley, A. M. Ganose, S. Sangiao, J. M. De Teresa, P. Manuel, D. D. Khalyavin, M. Walker, M. R. Lees, and R. I. Walton, Antiferromagnetism at $T > 500$ K in the layered hexagonal ruthenate $SrRu_2O_6$, Phys. Rev. B **92**, 104413 (2015).

[18] S. Streltsov, I. I. Mazin, and K. Foyevtsova, Localized itinerant electrons and unique magnetic properties of $SrRu_2O_6$, Phys. Rev. B **92**, 134408 (2015).

[19] S. V. Streltsov and D. I. Khomskii, Orbital physics in transition metal compounds: New trends, arXiv:1711.05409.

[20] F. Freund, S. C. Williams, R. D. Johnson, R. Coldea, P. Gegenwart, and A. Jesche, Single crystal growth from separated educts and its application to lithium transition-metal oxides, Sci. Rep. **6**, 35362 (2016).

[21] M. J. O'Malley, H. Verweij, and P. M. Woodward, Structure and properties of ordered Li_2IrO_3 and Li_2PtO_3, J. Solid State Chem. **181**, 1803 (2008).

[22] See Supplemental Material at http://link.aps.org/supplemental/10.1103/PhysRevB.97.020104 for details about sample preparation, experimental setup, and the results of additional calculations.

[23] F. D. Murnaghan, The compressibility of media under extreme pressures, Proc. Natl. Acad. Sci. USA **30**, 244 (1944).

[24] V. Hermann, J. Ebad-Allah, F. Freund, I. M. Pietsch, A. Jesche, A. A. Tsirlin, J. Deisenhofer, M. Hanfland, P. Gegenwart, and C. A. Kuntscher, High-pressure versus isoelectronic doping effect on the honeycomb iridate Na_2IrO_3, Phys. Rev. B **96**, 195137 (2017).

[25] S. Nishimoto, V. M. Katukuri, V. Yushankhai, H. Stoll, U. K. Rößler, L. Hozoi, I. Rousochatzakis, and J. van den Brink, Strongly frustrated triangular spin lattice emerging from triplet dimer formation in honeycomb Li_2IrO_3, Nat. Commun. **7**, 10273 (2016).

[26] S. M. Winter, Y. Li, H. O. Jeschke, and R. Valentí, Challenges in design of Kitaev materials: Magnetic interactions from competing energy scales, Phys. Rev. B **93**, 214431 (2016).

[27] G. Jackeli and D. I. Khomskii, Classical Dimers and Dimerized Superstructure in an Orbitally Degenerate Honeycomb Antiferromagnet, Phys. Rev. Lett. **100**, 147203 (2008).

[28] L. S. I. Veiga, M. Etter, K. Glazyrin, F. Sun, C. A. Escanhoela, G. Fabbris, J. R. L. Mardegan, P. S. Malavi, Y. Deng, P. P. Stavropoulos, H.-Y. Kee, W. G. Yang, M. van Veenendaal, J. S. Schilling, T. Takayama, H. Takagi, and D. Haskel, Pressure tuning of bond-directional exchange interactions and magnetic frustration in the hyperhoneycomb iridate β-Li_2IrO_3, Phys. Rev. B **96**, 140402 (2017).

[29] A. G. Petukhov, I. I. Mazin, L. Chioncel, and A. I. Lichtenstein, Correlated metals and the LDA + U method, Phys. Rev. B **67**, 153106 (2003).

[30] S. Manni, Sungkyun Choi, I. I. Mazin, R. Coldea, M. Altmeyer, H. O. Jeschke, R. Valentí, and P. Gegenwart, Effect of isoelectronic doping on the honeycomb-lattice iridate A_2IrO_3, Phys. Rev. B **89**, 245113 (2014).

[31] We note that without a further increase of the unit cell, only three antiferromagnetic patterns are possible: Néel ($\mathbf{q}$ =0), stripes, and zigzag (both $\mathbf{q}$ ={1,0} in plane), where the latter two are closer to the experimental wave vector. The choice between stripes and zigzag is rather arbitrary, and does not affect the final conclusions.

[32] T. Takayama, A. Kato, R. Dinnebier, J. Nuss, H. Kono, L. S. I. Veiga, G. Fabbris, D. Haskel, and H. Takagi, Hyperhoneycomb Iridate β-Li_2IrO_3 as a Platform for Kitaev Magnetism, Phys. Rev. Lett. **114**, 077202 (2015).

[33] N. P. Breznay, A. Ruiz, A. Frano, W. Bi, R. J. Birgeneau, D. Haskel, and J. G. Analytis, Resonant X-ray scattering reveals possible disappearance of magnetic order under hydrostatic pressure in the Kitaev candidate γ-Li_2IrO_3, Phys. Rev. B **96**, 020402(R) (2017).

[34] J. C. Wang, J. Terzic, T. F. Qi, Feng Ye, S. J. Yuan, S. Aswartham, S. V. Streltsov, D. I. Khomskii, R. K. Kaul, and G. Cao, Lattice-tuned magnetism of $Ru^{4+}(4d^4)$ ions in single crystals of the honeycomb ruthenates Li_2RuO_3 and Na_2RuO_3, Phys. Rev. B **90**, 161110 (2014).